ACS APPLIED NANO MATERIALS

www.acsanm.org Article

Agarose-Based Fluorescent Waveguide with Embedded Silica Nanoparticle–Carbon Nanodot Hybrids for pH Sensing

Francesco Amato, Marco César Prado Soares, Thiago Destri Cabral, Eric Fujiwara, Cristiano Monteiro de Barros Cordeiro, Alejandro Criado, Maurizio Prato,* and Julio Roberto Bartoli*

Cite This: *ACS Appl. Nano Mater.* 2021, 4, 9738–9751 Read Online

ACCESS | Metrics & More | Article Recommendations | Supporting Information

ABSTRACT: The fabrication of a biodegradable and fluorescent cylindrical waveguide with doped hybrid nanoparticles (silica–carbon nanodots) is reported. The fluorescent hybrids were obtained by coupling amino-functionalized fumed silica nanoparticles with the carboxylic acid surface groups of amorphous carbon nanodots obtained from the thermolysis of citric acid. The hybrid nanoparticles present diameters lower than 10 nm, maximum fluorescence at 465 nm, and excitation-wavelength-dependent behavior. They were occluded into an agarose matrix, providing a low-cost and easily scalable sensor capable of detecting pH variations with maximum sensitivity of 5.61 nm/(pH unit) when excited by a 403 nm UV light-emitting diode (LED).

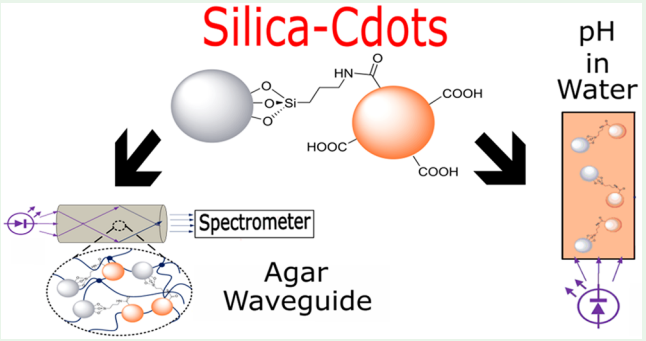

KEYWORDS: *carbon nanodots, fumed silica, hybrid nanoparticles, agarose, pH detection, biodegradable fluorescent waveguide, polymeric optical fiber*

INTRODUCTION

Despite all of the different techniques and fabrication materials available for the production of optical fibers, waveguides, and optical sensors, the development of devices with lower costs and minor difficulties of fabrication, signal interpretation, and practicality is still needed.[1] An important technological gap, on the other hand, is to combine the solution of these problems with the environmental point of view, producing biodegradable devices and using less aggressive processes. In this context, the use of biocompatible hydrogels arises as a promising methodology for manufacturing photonic platforms. This approach allows obtaining implantable sensors and reducing undesirable effects of the traditional silica optical fibers, such as the formation of sharp points that may inflame the implant region. For instance, silk-based hydrogels have already been used for fabricating thin films, diffraction gratings, and organic photonic crystals.[2,3]

Hydrogel-based waveguides combine, then, the electromagnetic interference shielding with the possibility of miniaturization, allowing the detection of different parameters with high sensitivity.[4] They usually explore the properties of hydrogels in suffering volumetric variations as a response to different parameters, including pH, temperature, ionic strength, and concentration of analytes, such as glucose, proteins, and DNA. These different potential applications in industrial biotechnology, environmental monitoring, and biosensing[1,5,6] can be also increased by doping the polymeric matrix with luminous agents.

The doping strategy is based on the variation of the pattern of the light transmitted by the waveguide due to luminescence and other light–matter interaction phenomena. Studies have shown, for example, the possibility of producing step-index cylindrical optical fibers by coating a poly(ethylene glycol) (PEG) core with an alginate layer. These materials allowed the guiding of light inside living tissues and were doped with fluorophores and Au nanoparticles. Both types of doping allowed the sensor to selectively detect avidin.[7] A PEG optical fiber was also doped with functionalized CdTe quantum dots (QDs) for monitoring Fe^{3+}.[8] Meantime, practical applications of these devices are still limited by the fact that inorganic nanoparticles such as the semiconductor QDs usually present high toxicity,[9] which can be overcome by their substitution by carbon nanodots (CDs).[10]

These carbon nanodots are materials emerging from the family of carbon nanotechnology (as well as graphene, fullerene, and carbon nanotubes), which present quasi-spherical morphology and sizes lower than 10 nm.[10,11] They are constituted by a carbonaceous core with plenty of functional groups on the surface, such as hydroxyls, amines, and carboxylic acids, allowing their solubility in polar solvents. The peculiar behavior of carbon

Received: July 23, 2021
Accepted: August 9, 2021
Published: August 20, 2021

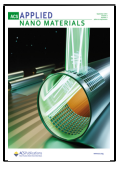

nanodots is their fluorescence, which arises from molecular domains that are formed during the synthesis that is carried out at high temperature.[10−17]

This luminescent behavior of CDs may be modulated by different factors, especially the excitation wavelength,[12] pH,[19] and solvent used.[20] Moreover, the surroundings of the particles are responsible for the stabilization of the fluorophore electronic states, and red-shifted emissions are expected when the neighboring particles stabilize such states (solvatochromic effect).[21] Due to these unique peculiarities, CDs find applications into several fields, such as biomarking, bioimaging, drug delivery, optoelectronics [in which they can be used for manufacturing light-emitting diodes (LEDs) with controlled emission wavelength],[14,17] covalent asymmetric catalysis,[22] photocatalysis, renewable energies,[14] luminescence down shifting, and solar concentrator devices.[23−25]

The advantages of CDs compared to inorganic QDs (considered superior fluorescence emitters) also include the fact that they are low-cost and environmentally safe materials[10] and show good biological and biocompatibility properties, being excreted in urine.[14,15] Moreover, they present chemical robustness and high solubility in water and are easily doped and chemically modified.[16] CDs have been produced with different photonic properties that rely on the particular routes and chemical precursors applied.[24,26,27]

Some examples of synthesis include the one of Arcudi et al.,[11] who obtained small and highly fluorescent nitrogen-doped carbon nanodots (NCNDs) using a bottom-up approach by microwave-assisted hydrothermal carbonization, starting from inexpensive L-arginine and ethylenediamine. The study by Martindale et al.[28] has shown the application of citric acid CDs in the light-driven fabrication of chemical products, performing an artificial photosynthesis by preparing a photocatalytic hybrid system (CD−NiP) for solar H_2 production.

Also, previous studies showed that CDs can be easily fabricated in domestic microwave ovens using sugar cane syrup, a low-cost and renewable source.[29] Boobalan et al.[30] obtained CDs by hydrothermal synthesis using another green source, oyster mushroom. The fabricated material is capable of selectively sensing Pb^{2+} ions in aqueous solutions and presents antibacterial and anticancer activity. CDs may even be doped with Mn by submitting mixtures of sodium citrate, citric acid, and manganese(II) carbonate to hydrothermal treatment (195 °C, 2 h). These Mn-doped particles present ultrahigh quantum yield of luminescence and may be used to selectively detect Hg^{2+} ions in water.[31] A detailed review describing synthetic routes for obtaining CDs from both artificial and natural sources (such as silk and grass), as well as some applications already demonstrated for them, was recently published and is referred to for those interested in this particular topic.[32]

In this study, carboxylic acid carbon nanodots, obtained from the thermolysis of citric acid, were used to produce amorphous nanohybrids by coupling CDs to silica and were tested for pH detection. Then, we occluded these nanoparticles into agarose to produce a waveguide with intrinsic fluorescence, obtaining a device suitable for pH sensing. The use of the hybrids instead of the net CDs is related to their physical properties: since the hybrid nanoparticles present slightly higher densities and are less hygroscopic, they are easier to manipulate under the larger scales of the hydrogel.

The chemical attainment of the silicon dioxide−CD hybrids was based on the report from An et al.[33] These authors described a method to assemble silica nanoparticles into silicon wafers through the direct amidation between the amine group of the silicon surface and the carboxyl groups of modified silica nanoparticles. More recently, a second route was proposed by An et al.,[34] which consists of the hydrothermal synthesis of hybrids of carbon dots/SiO_2 and gold nanoclusters. They showed that the particles were suitable for detecting Ag^+ in water.

In a very comprehensive review about the incorporation of CDs into different polymer and ceramic matrixes, Jiang et al.[35] concluded that matrixes with a plethora of sites containing hydroxyl and other oxidized groups can stabilize the excited state of the carbon dots. In particular, the authors highlighted the composites of poly(vinyl alcohol) (PVA), in which hydrogel networks may form numerous hydrogen bonds with the polar groups of CDs, stabilizing the emission. Thus, we selected agar as the material for fabricating the waveguides because we expected a similar stabilization of the CDs' emissions related to the presence of the C−OH and C−O−C groups of agarose[36] and because of the large availability of this material, which may be usually bought at local markets in food grade. Agar also shows satisfactory mechanical properties for many biomedical and monitoring applications, with the possibility of thermal curing. This last characteristic facilitates the manufacturing and reduces costs, since no curing agent or equipment is needed.[8,35,36] Finally, ions and molecules from the external environment may diffuse through the matrix, allowing the sensing.[8,36]

Even though some studies have already reported pH assessment based on the use of fluorescent nanoparticles, there are important peculiarities that distinguish them from this research. These differences include the synthetic routes and chemical identities of the obtained particles and difficulties and complexity of the interrogation strategy or of their integration and application in biosystems. For instance, Wang et al.[37] hydrothermally synthesized crystalline (graphitic) CDs by introducing a solution of 1,2,4-triaminobenzene and NaOH into an autoclave (heating under 180 °C for 12 h). The dots were first dispersed in water to be used for the colorimetric analysis of pH: the solutions were excited with either daylight or ultraviolet (UV) light and analyzed by UV−vis and fluorescence spectroscopy. Then, the particles were loaded into pH test papers to obtain a colorimetric pH sensor interrogated by image processing. Not only is pH paper not as easily integrated into biosystems as hydrogels, but it is also not a device designed to conduct light. In turn, this approach is similar to the one used by Zhang et al.,[38] who obtained core−shell CDs from the hydrothermal treatment of an aqueous solution of 5-amino-1,10-phenanthroline and citric acid (heating in a Teflon-lined 50 mL autoclave under 200 °C, over 7 h).

After being purified with a dialysis membrane, the particles were applied to color-based pH detection by dispersing them in water or by printing that solution into filter papers, further stuck onto A4 papers. As in the study from Wang et al.,[37] the samples were excited by either sunlight or UV light, and then image processing was used to obtain the luminescence intensity. Finally, the intensity was correlated to the pH through calibration curves.

Both studies[37,38] experience some concerns, as the colorimetric analysis of samples' images may be influenced by external factors, for example, the variation of the camera's position or of the object's location, oscillations of the environmental light or of the brightness level of the recorded images, sensitivity and resolution of the image detector, focal length of the lens, and particular methods chosen for image calibration and for the

https://doi.org/10.1021/acsanm.1c02127
ACS Appl. Nano Mater. 2021, 4, 9738−9751

Scheme 1. Synthesis Routes of α-CDs, Amino-Terminated SiO_2 Nanoparticles, and Hybrids of α-CDs Coupled to a-SiO_2

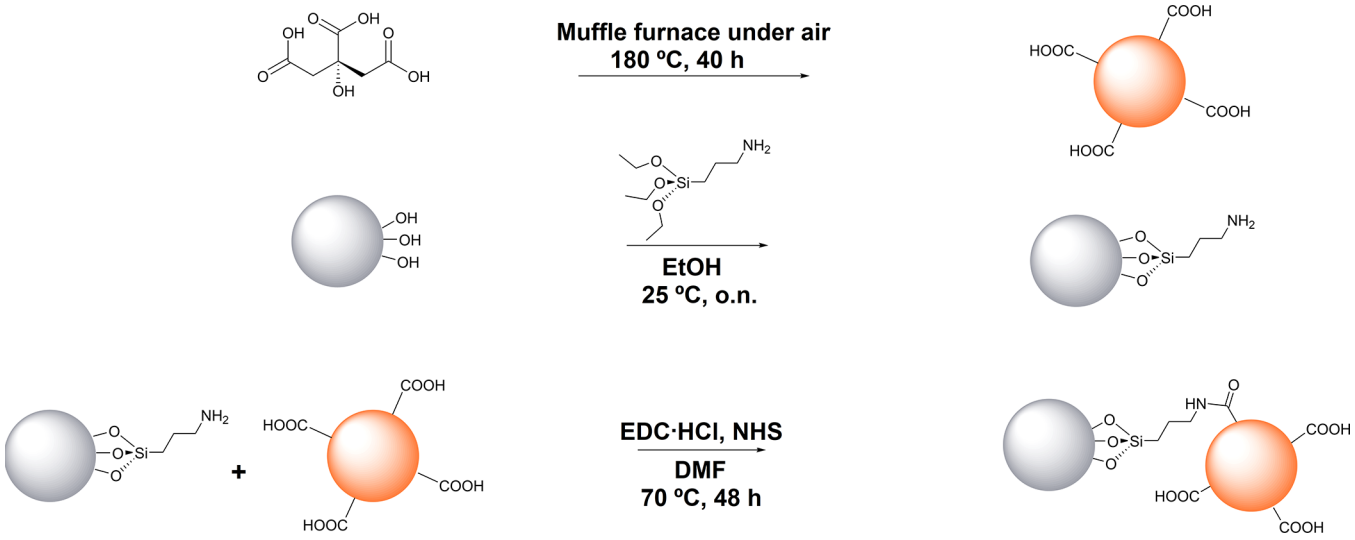

image dewarping.[39,40] Additionally, the detection often requires the removal of samples from the analyzed medium (for off-line analysis), as well as constant recalibration procedures when applying the sensor to practical applications. This is not observed when an optical waveguide sensor is used, as in this study. That is because wavelength interrogation and other optical fiber sensing technologies are usually robust regarding the above-mentioned factors.[39,40]

An important final example to be mentioned is the fluorescent pH sensor reported by Chen et al.[41] They fabricated inorganic CdTe QDs (particles with environmental and safety issues), and then mixed them with CDs hydrothermally obtained from an aqueous solution of chitosan and hydrogen peroxide (heating under 180 °C for 5 h). The CDs−QDs dispersions were used in the ratiometric detection of pHs ranging from 3.0 to 11.0. Samples of the nanoparticles under different pHs were collected and introduced into quartz cuvettes to be analyzed in a fluorometer. Then, the ratio between the maximum intensity peaks corresponding to each of the nanoparticles was obtained and correlated to the pH. Again, this is a system that is not easily integrated to simple standard optical instrumentation. Besides, it does not show either the possibility of on-site monitoring or the biocompatibility characteristic of the hydrogel.

Therefore, herein we report a simple and scalable method for obtaining an innovative green and disposable optical pH sensor. The sensor was constructed as a cylindrical optical waveguide made by a biodegradable and fluorescent agarose doped with hybrid nanoparticles of silica−carbon nanodots (silica−Cdots).

EXPERIMENTAL SECTION

Silica−Cdots Nanohybrid Synthesis. Carboxylic acid terminated carbon nanodots, denominated here as α-CDs, were synthesized from the thermolysis of 200 g of citric acid (Fluka, 99.5%). The synthesis was performed in a muffle furnace under atmospheric air at 180 °C for 40 h, as reported by Martindale et al.[28] A yellow-orange powder was obtained after the thermal treatment, as represented in Scheme 1 and shown in Figure S1 (Supporting Information).

Amino-functionalized silica nanoparticles (a-SiO_2), in their turn, were prepared from commercial amorphous fumed silica nanoparticles treated with 3-aminopropyltriethoxysilane (APTES). Briefly, 206 mg of commercial fumed nanosilica (Aerosil 300, synthetic amorphous silica, average primary particle size ∼7 nm, Evonik) previously dried for 2 days at 105 °C was added to ethanol (50 mL), and the mixture was stirred for 3 min. Then, APTES (5 mL, Sigma-Aldrich) was added and sonicated for 5 min, and the dispersion was stirred at room temperature (r.t.) and overnight (o.n.). After this step, the mixture was purified by centrifugation, and was then dispersed in ethanol (procedure repeated three times). The dispersion was lyophilized, leading to the a-SiO_2 nanoparticles. Then, the hybrid silica−Cdots were synthesized through an amidic coupling reaction between a-SiO_2 and carboxyl-rich α-CD, as also depicted in Scheme 1.

For this last synthesis, 223 mg of α-CDs dispersed in 10 mL of anhydrous dimethylformamide (DMF) was mixed with 50 mg of a-SiO_2 under an inert environment (Ar) and with 200 mg (1.04 mmol) of 1-ethyl-3-(3-(dimethylamino)propyl) carbodiimide hydrochloride (EDC·HCl, Alfa Aesar). An amount of 120 mg (1.04 mmol) of *N*-hydroxysuccinimide (NHS, Sigma-Aldrich) was also added. Finally, this mixture was sonicated for 10 s and stirred at 70 °C for 2 days at r.t. DMF was removed through azeotropic distillation with toluene under reduced pressure, and Milli-Q water was added. In order to purify the product, two cycles of centrifugation (20 min at 3000 rpm) were performed, followed by freeze-drying. The changes of color of the three dried materials (a-SiO_2, α-CD, and silica−Cdots) are shown in Figure S1.

Hybrids Physicochemical Characterization. The images of the a-SiO_2, α-CD, and silica−Cdots nanoparticles were obtained by transmission electron microscopy (TEM) on a Philips EM 208 (FEI, operation under 100 kV, magnification of 50×10^3 times). The samples were prepared by dropping the aqueous nanoparticles dispersion onto a carbon-coated copper grid. Additional TEM analyses were performed for the α-CD nanoparticles using a field-emission gun (FEG-TEM) JEOL JEM-2100F (80−200 kV), ultrahigh-resolution pole piece, under low electron dose conditions and equipped with a TVIPS F216 CMOS camera (2048 × 2048 pixels resolution). The α-CD samples were negative-stained with ammonium molybdate, which allows the formation of a uniform, consistent, and high-contrast staining. The specimen preparation was as follows: α-CD powder was diluted in 30% (v/v) DMF (1/3 DMF: 2/3 H_2O), sonicated for 90 min, and afterward centrifuged with a small table centrifuge for 10 min, using the supernatant as a sample and negative-staining with 2% ammonium molybdate. Conventional bright-field TEM images were acquired for the α-CD negative-stained specimens.

The particles were physicochemically characterized by the following techniques:

X-ray diffratometry (XRD) using a Philips X'pert PRO automatic diffractometer operating at 40 kV and 40 mA, a secondary monochromator with Cu Kα radiation (λ = 1.5418 Å), a PIXcel solid-state detector, a scan speed 0.01°/s, and at room temperature;

https://doi.org/10.1021/acsanm.1c02127
ACS Appl. Nano Mater. 2021, 4, 9738−9751

Fourier transform infrared spectroscopy (FT-IR) using a 2000 spectrometer (PerkinElmer); transmission spectra of the powder samples were recorded using KBr and resolutions of 3 and 10 scans;

X-ray photoelectron spectroscopy (XPS), with a SPECS Sage HR 100 spectrometer equipped with a 100 mm mean radius PHOIBOS analyzer (SPECS Surface Nano Analysis); a Mg Kα X-ray source was used, and XPS data fitting was carried out using CasaXPS software;

Raman spectroscopy using a Renishaw in Via Raman microscope at 532, 633, and 785 nm laser lines, 10% laser power, and a 10 s exposition time;

Thermogravimetric analysis (TGA) using a TGA Q500 (TA Instruments), performed by imposing an isotherm at 100 °C for 20 min, followed by a ramp of 10 °C/min under N_2 at flow rates of 90 and 10 mL/min on the sample and balance, respectively.

The aqueous dispersions of nanoparticles also had their photoluminescence (PL) spectra at room temperature observed with a Cary Ellipse−Varian fluorescence spectrophotometer (Agilent Technologies) at excitation wavelengths from 300 to 430 nm, a 600 nm/min scan speed, and excitation and emission slits of 5 nm.

pH Monitoring with Hybrids Dispersed in Water. Due to the presence of carboxylic groups, the possibility of applying the hybrids for pH assessment was evaluated. In this analysis, a dispersion containing 1.2% (m/m) of silica−Cdots (~12 g/L) in deionized (DI) water was progressively alkalinized by the drop-by-drop addition of 0.01 M NaOH. The aqueous solution containing silica−Cdots showed a pH of 4.3 when the hybrids were added, reducing the pH of the deionized water and becoming the initial pH. After each addition, the sample had its pH quantified, was introduced into a cuvette (length of 1 cm), and was excited by a 403 nm LED with a full width at half-maximum (fwhm) of 12.2 nm. Then, the fluorescence spectrum was recorded with a hand-held spectrometer (HR4000, resolution of 0.3 nm, Ocean Optics) to obtain the wavelength of maximum fluorescence. After raising the pH to ~12, the opposite procedure was performed. The pH was reduced until it was ~2 by adding 0.01 M HCl to the dispersion (drop-by-drop addition), and the luminescence spectra were collected analogously.

The nanohybrid concentration of 1.2% (m/m) was chosen for providing an adequate balance between the total fluorescence intensity and the LED attenuation by the particles. This particular light source (403 nm) was selected by taking into account aspects of optical power, wavelength, cost, and safety. A detailed discussion about the advantages obtained using this kind of LED is given in the Supporting Information.

Agar Cylindrical Waveguide Fabrication and pH Sensing. Two types of cylinders were prepared by gelling precursor solutions containing agarose in DI water. The first solution contained 300.0 mg of agarose (food grade, acquired in a local market) and 31.0 mg of hybrids (silica−Cdots) dispersed in 10 mL of water, resulting in concentrations of 30.0 g/L (agarose) and 3.10 g/L (hybrids). The second solution was fabricated for comparison: it contained the same concentration of agarose in DI water (30.0 g/L), but no nanoparticles.

The solutions were heated close to their boiling points for initiating the agarose thermal-curing process. This process consists of a cold-setting mechanism related to the formation of double-helixes between the polymeric chains. After being heated above ~85 °C, cross-links are observed between the macromolecules, resulting in the gel formation when the system is cooled. Thus, this reticulation is favored by imposing lower cold temperatures during the cooling step.[36]

So, immediately after the first signs of boiling (i.e., formation of small bubbles and of visible aqueous vapor above the liquid surface), the precursor dispersions were introduced into 3D-printed cylindrical molds (7 mm inner diameter) made of glycol-modified poly(ethylene terephthalate) (PETG) filament (3D printer Ultimaker 2+, Ultimaker BV). The molds were sealed on their end-faces, and left o.n. in the refrigerator at ~10 °C for curing. This process forms hydrogels with the same geometry as the internal mold walls, and these hydrogels can be easily demolded by removing the sealing and the two cylinder's bases (the mold caps are pluggable). After removing the sealing, the hydrogel is left to dry under ambient conditions, so the loss of water diminishes its diameter and provides the loss of contact with the inner walls. After being removed, the formed materials are again put in contact with DI water for recovering the original diameter of 6 mm.

The refractive indexes (RIs) of both the agar and the agar with occluded hybrids were evaluated with a MISCO PA 202 refractometer (Palm Abbe), with a 589 nm high-precision LED (resolution of 10^{-4} nm). All samples were measured at ~25 °C and room atmosphere. For this, small volumes of the preheated precursor solutions (heated until boiling) were dropped on the sample window. The reading of the RI was performed after the curing and thermal stabilization of the system at 25 °C. The obtained refractive indexes were n = 1.3334, which is very close to the DI water's index (n = 1.3330, evaluated using the same equipment). This is due to the high adsorption of H_2O on the hydrophilic polymers and on the hybrids' surfaces. This value is also higher than the air's ($n \approx 1$), so light may be guided through total internal reflectance, as in conventional optical fibers[18] (this is represented in Scheme 2).

Scheme 2. Agarose Waveguide Doped with the Hybrids

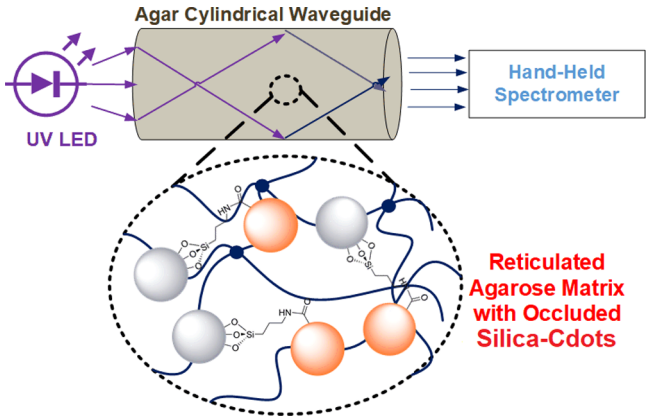

As detailed in the Supporting Information, a numerical aperture (NA, a measurement of the efficiency of guiding) of 0.882 was obtained for the transmission of light by the doped agar surrounded by air (eq S1). Once this value is higher than zero, it guarantees the guidance of light. The operation of the waveguide immersed in water is also possible, but the guiding efficiency would be lower: the application of eq S1 to this second situation results in NA = 0.054.

The transmission spectra of both waveguides (doped agarose used as the pH sensor and the net agar used as the reference) were analyzed by exciting them with a supercontinuum laser (SuperK Compact, NKT Photonics) in one extremity and collecting the light at the end-face with a spectrometer.

Finally, the waveguides containing occluded silica−Cdots were submitted to the same pH test previously performed with the aqueous dispersions of nanoparticles (i.e., the irradiation with a 403 nm LED, followed by the analysis of the fluorescence spectra).

The experimental setup remained basically the same (only the cuvette was removed) and took advantage of the material's very high affinity with water: first, the waveguide was kept in the aqueous medium, under stirring and in a given pH. Due to the high hydrophilicity of both the agar and the hybrids, the intumescence degree (and, consequently, the solution's pH) takes no longer than 30 s to stabilize. At this moment, no more variation of the waveguide's diameter could be observed under the naked eye. Then, the pH reading got stable, and the agar waveguide was rapidly removed from the aqueous medium. It was put into the same place previously occupied by the cuvette and was stimulated by the LED. The light emerging from both the end-face and from the air−agar side interface was collected and analyzed. After each measurement, the waveguide was returned to the aqueous medium for repeating the process under a different pH. Again, the pH was first raised to ~12 by adding 0.01 M NaOH, and then it was reduced by dropping 0.01 M HCl.

https://doi.org/10.1021/acsanm.1c02127
ACS Appl. Nano Mater. 2021, 4, 9738−9751

The pH limits (from 2 to 12) applied to both the tests with the aqueous dispersion and with the doped waveguide were chosen to include the range commonly observed in living organisms and biochemical systems (generally from 4 to 8). In addition, these pHs do not present security risks for the experimenters and mitigate the risks of damaging the agarose matrixes or the optical instruments.[42] All of the pH experiments were performed at room temperature (constant, ~25 °C) and in an air atmosphere.

RESULTS AND DISCUSSION

Carboxylic acid terminated carbon nanodots (α-CDs) were obtained from the thermolysis of citric acid.[28] After that, they were coupled to amino-functionalized silica nanoparticles (a-SiO_2) to obtain a silica−Cdots nanocomposite (Scheme 1). As described in Supporting Information, the UV−vis absorption spectra of both the α-CDs and of the silica−Cdots (Figure S2) show maximum absorbance at 300 nm, corresponding to the $\pi \rightarrow \pi^*$ transition of the sp^2 carbons of the CDs cores. The α-CDs show a shoulder at 360−390 nm with a tail that extends to the visible range, assigned to the $n \rightarrow \pi^*$ transitions involving the electron lone pairs of the carboxylic surface groups. On the other hand, silica−Cdots showed a relative increase in UV−vis absorption from 350 to 600 nm and no shoulder, compared to the α-CDs.

The nanoparticles were characterized by TEM, FEG-TEM, FT-IR, Raman, XPS, and TGA, and their PL spectra were assessed. Then, aqueous dispersion of the hybrids were illuminated with a 403 nm LED, and the fluorescence emissions were analyzed to retrieve the pH. Finally, the particles were occluded into agarose matrixes to fabricate a biodegradable waveguide for pH sensing (Scheme 2).

Hybrids and Carbon Nanodots Characterization. The TEM image of fumed silica−carbon nanodots hybrids (silica−Cdots), Figure 1, shows aggregates (~50 nm) formed by primary amorphous particles with sizes of around 6 nm. Since the carboxylic acid carbon nanodots (α-CDs) are amorphous, they are hardly identified by TEM analysis. Nevertheless, variations in diameter and morphology were observed by TEM for the α-CDs, a-SiO_2, and silica−Cdots particles (Figures S3−S5). The sizes of α-CDs found are in accordance with Martindale et al.,[28] who obtained an average size of 6.8 ± 2.3 nm for amorphous carboxylic acid carbon nanodots and a relatively broad size distribution. It is also in accordance with the average primary particle size reported for the used amorphous fumed silica (Aerosil 300), 7 nm measured through dynamic light scattering.[43]

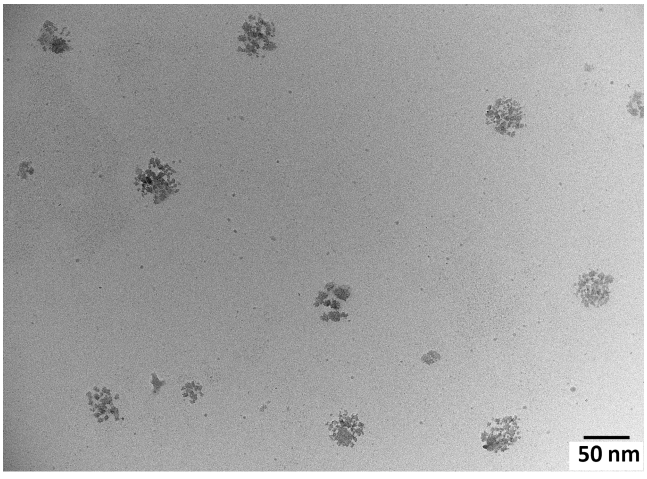

Figure 1. TEM images of silica−Cdots aggregates (~50 nm) and primary particles (~6 nm).

The TEM images of the α-CDs (Figure S3A) showed dispersed primary, spherical, amorphous nanoparticles with diameters of around 6 nm. The images of amino-terminated silica, a-SiO_2 (Figure S4), showed dispersed primary particles and aggregates of around 6 and 100 nm, respectively. The primary particles of a fumed silica do not occur just isolated or evenly dispersed; they also merge to form aggregates.[43] They are held together because of weak interactions, such as van der Waals forces or hydrogen bonds. Consequently, amorphous silica−Cdots hybrids are not seen as dispersed as α-CDs (Figure S5), showing overlapping or agglomeration of particle aggregates (100−300 nm) and primary particles (~6 nm).

FEG-TEM high-resolution images of carbon nanodots (α-CD) were also obtained, after negative staining of the nanoparticles in an attempt to make the morphology visible. They are seen as dark bloblike spots embedded in the gray background (Figure S3, parts B and C). No lattice fringes or contrast lines were observed, as expected for amorphous particles. The appearance is typical for objects composed of very light elements having been negatively stained with ammonium molybdate. The carbon nanodots appear in sizes between approximately 4 and 10 nm. Very tiny white dots that become visible everywhere in the images are considered to be grains derived from ammonium molybdate. Brighter gray islands, much bigger than the dark blobs, sometimes also containing even bright tiny spots, could be formed by sodium. Energy-dispersive X-ray spectroscopy (EDX) analysis confirmed that Na is present in the TEM sample. The origin of this Na is likely from the staining solution containing Na from pH adjustments.

Although it is difficult to distinguish carbon dots in the TEM images of the silica−Cdots, due to their amorphous nature, their presence was confirmed by XRD, XPS, FT-IR-ATR, and Raman analyses and TGA, presented below.

SiO_2: the amorphous halo of the fumed SiO_2 is observed at around $2\theta = 21.5°$.

α-CD: the amorphous halo observed around $2\theta = 18.5°$ could be due to some oxidized graphitic species; in turn the presence of graphitic species is imperceptible, as only a very smooth tail is observed around $2\theta = 30°$. Diffraction patterns for graphite and oxidized graphite are expected with strong reflections at 27° and 16°, respectively.

a-SiO_2: two amorphous halos are observed around $2\theta = 8.5°$ and $2\theta = 21.5°$ due to the amino group and SiO_2, respectively.

Silica−Cdots: the amorphous halo of SiO_2 (~21.5°) overlaps the α-CD halo (shoulder at ~18.5°), and some contribution of the amino group is observed (~8.5°).

The FT-IR spectra for the SiO_2, a-SiO_2, α-CDs, and silica−Cdots nanoparticles are shown in Figure 2. A complete description of assigned bands, in turn, is provided in the Supporting Information, Figures S6−S8. The XPS and TGA results are also shown in the Supporting Information (Figures S9−S12).

The spectra presented in Figure 2 and Figure S6 demonstrate the amino functionalization of the SiO_2 particles. The spectrum of silica exhibits typical absorption bands at the wavenumbers of 473 cm^{-1}, due to bending motions of Si−O, 1107 and 804 cm^{-1}, assigned to the asymmetric and symmetric stretching of the Si−

https://doi.org/10.1021/acsanm.1c02127
ACS Appl. Nano Mater. 2021, 4, 9738−9751

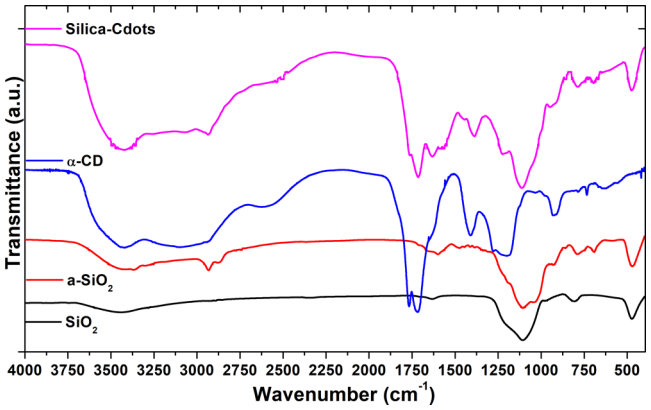

Figure 2. FT-IR spectra collected for fumed silica, amino-functionalized silica, α-CDs, and silica−Cdots.

O−Si bonds, respectively, and the 3437 cm^{-1} broad band due to Si−OH and −OH stretching.[44,45] There is also a band around 1630 cm^{-1}, which is due to the scissor bending vibration of the −OH groups of adsorbed molecular water.[46] The FT-IR spectrum of the amino-functionalized silica (a-SiO_2) reveals the presence of the C and N groups expected from the reaction between SiO_2 and APTES (Scheme 1). Typical amine vibrational absorption bands are observed at 690 cm^{-1} assigned to N−H wagging, 1044 cm^{-1} assigned to C−N stretching, 1445 and 1600 cm^{-1} assigned to N−H bending, and 2881−2932 cm^{-1} assigned to C−H stretching. Again, the presence of molecular water originates an −OH bending band around 1630 cm^{-1}.[44−46]

The carbon nanodots' spectrum displays typical carboxylic acids vibrational absorption bands. There is a very broad and intense O−H stretching absorption in the region of 3300−2500 cm^{-1}, with a long-wavenumber side of the O−H band due to the overtone of the fundamental bands at high wavenumbers. The intense stretching vibrations bands of C═O are located in the region of 1767−1718 cm^{-1}. The absorption band at 1409 cm^{-1} is referred to the bending vibration of C−O−H, the band at 1278−1197 cm^{-1} is due to the stretching vibrations of C−O, the band at 925 cm^{-1} is due to the out-of-plane bending vibration of O−H, and the −OH bending of water is present at ∼1630 cm^{-1}.[44−46]

Once the hybrids are expected to show both the groups from the amino-functionalized silica and from the carbon dots, the silica−Cdots FT-IR spectrum was compared with the data collected for the a-SiO_2 (Figure S7) and for the α-CDs (Figure S8). Indeed, the characteristic absorption bands of the amino-silica and of the carboxylic acids are observed in the silica−Cdots spectrum (Figure 2, Figure S7, and Figure S8): Si−O and Si−O−Si (473 and 804 cm^{-1}); C−O at 1222 cm^{-1}, overlapped with the Si−O−Si at 1107 cm^{-1}; C−O−H, C═O, and C−H at 1386 cm^{-1}, 1715 and 2930 cm^{-1}, respectively. Besides, the intense band of the Si−O−Si (1107 cm^{-1}) has a shoulder at 1044 cm^{-1} due to the C−N stretching.[44−46] When comparing Figure 2 and Figure S7 to Figure S8, the OH stretching band (around 3400 cm^{-1}) appears to be more intense and broader after the coupling reaction.

Raman spectra of α-CDs and silica−Cdots nanoparticles (Figure S14) did not show any scattering signal, and only fluorescence effects were observed. The broad luminescence arises from the strong PL emission of carbon nanodots excited at the wavelength of 532 nm, and even at 633 and 785 nm, laser lines also used in this study, which could cover any likely very weak Raman band. In turn, the non-noticeable D or G bands in the Raman spectra indicate disordered carbon atoms, a further evidence of the amorphous morphology of the α-CDs and silica−Cdots nanoparticles.

The TGA is shown in Figure S9. It detected almost no mass variation for SiO_2. This was expected, since the applied thermal range is inferior than the temperatures required for silica phase transitions and also because there are no organic groups to degrade.[47,48] On the other hand, TGA assessed the significant organic content of the silica after the amino functionalization (a-SiO_2) and after the coupling reaction with the carbon nanodots (silica−Cdots). The TGA profile of silica−Cdots shows an event between ∼140 and 350 °C, which is due to the thermal degradation of amorphous α-CDs.[26,30] Both the a-SiO_2 and the silica−Cdots show mass losses between ∼350 and 560 °C that are related to the decomposition of alkyl-amino groups. No additional mass variations were found after 650 °C. The percent residual masses at 750 °C were around 97%, 60%, and 40% for the SiO_2, a-SiO_2, and silica−Cdots nanoparticles, respectively. The relative amounts of SiO_2 and α-CDs in the hybrid nanoparticles were around 40% and 25%, respectively; thus, the α-CDs/SiO_2 mass ratio was estimated at ∼60%.

In addition, XPS analysis was employed to provide the chemical composition of a-SiO_2 and α-CDs and, thus, to evidence the formation of silica−Cdots. The XPS spectra and atomic quantification of a-SiO_2, α-CDs, and silica−Cdots are shown in Figures S10−S12 and Table S1, respectively. The spectra of the nanoparticles are characterized by the chemical moieties C−C, C−O, C−N, C−NH_2^+, and Si−O for a-SiO_2 (Figure S10B−E), C−C, C═C, C−O, and C═O for α-CDs (Figure S11, parts B and C), and C−C, C═C, C−O, C═O, N−C, N═C, NH−(C═O), and Si−O for silica−Cdots (Figure S12B−E).

As expected, N (4.3%) and Si atoms (1.5%) were detected in the hybrid sample silica−Cdots. There is a significant increase in the C/Si ratio on the surface of the hybrids (49.5) compared to the a-SiO_2 (1.6), which is 30 times lower. This indicates that the number of silicon-based particles is lower in the CDs when compared to the hybrids and/or that these silicon particles are located at the core of the system. In addition, the deconvolution of the Si 2p core level showed two peaks at 101.9 and 102.3 eV, which correspond to the Si−O bond in the SiO_2 structure (Figure S12E).[49] Besides, the deconvoluted N 1s core level exhibited an intense peak at 399.5 eV, which can be assigned to the amide bond NH−(C═O) between the amino-functionalized silica and the carboxylic acid surface groups of the carbon nanodots (Figure S12C).[50] Thus, the XPS analysis confirmed the coupling reaction between a-SiO_2 and α-CDs resulting in the silica−Cdots hybrids.

Tougaard[51] revisited an issue in quantitative XPS analysis based solely on measured peak intensities. The intensity attenuation could be a consequence of the distance traveled by the photoelectron in the sample, which is an issue for samples where the atomic concentration varies over the outermost ∼5 nm. Indeed, this is the depth range for many of the nanostructures such as the primary particles of the silica−Cdots hybrids. Therefore, the combining of these XPS surface results with the bulk information from KBr FT-IR and TGA corroborates the coupling reaction between a-SiO_2 and α-CDs. In short, the hybrids presented both intense Si−O−Si and C═O FT-IR bands (typical of α-CDs) and around 40% and 25% of SiO_2 and α-CDs relative mass, respectively.

https://doi.org/10.1021/acsanm.1c02127
ACS Appl. Nano Mater. 2021, 4, 9738−9751

The PL emission spectra of α-CDs recorded in water (Figure 3A) show a maximum emission at 465 nm when the sample is

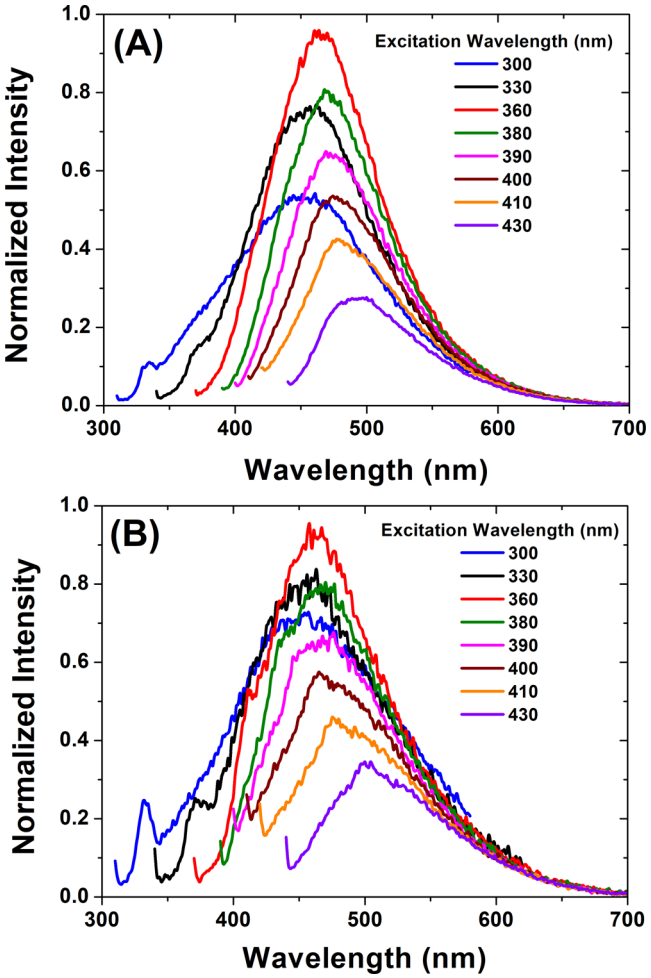

Figure 3. Fluorescence spectra of (A) α-CD and (B) silica−Cdots.

irradiated at 360 nm. When the excitation wavelength changed from 360 to 440 nm, an emission dependency with the excitation was observed with a concomitant loss of intensity. The PL spectra of the silica−Cdots in water (Figure 3B), in turn, show approximately the same behavior. The emission is dependent on the excitation wavelength, but the coupling caused an increase in the noise of the intensity signal. The maximum fluorescence intensity is still observed when the sample is excited by 360 nm (and still corresponds to the emission at 465 nm). It indicates that there is no loss of the stability of the excited state of the fluorescent agent caused by the silica coupling.[21] Moreover, the fluorescence emission peak of the hybrids shifts from 465 to 513 nm (green) when the excitation changes from 360 to 430 nm. The peak intensities also decrease as they red-shift, a behavior previously observed for other CDs.[28,29] Again, the organic groups present on the surface of the CDs significantly affect the fluorescence properties.[11,28]

pH Monitoring with Silica−Cdots Hybrids Dispersed in Water. The use of silica−Cdots hybrids for pH monitoring tests has advantages because they are easy-to-handle powders, as they are less hygroscopic than α-CDs. Besides, silica-based nanoparticles doped with fluorophores are interesting hybrid nanosystems that intrinsically combine the mechanical properties of silica with the optoelectronic properties of carbon nanodots. In particular, the use of hybrids can favor the large-scale manufacture of fluorescent agarose waveguides as pH sensors. In turn, the fluorescence intensity measurements of α-CDs are relatively smaller than those of the hybrids (Figure 3, parts A and B), a trend observed at other wavelengths used (300−430 nm). Considering the excitations in which the hybrids were slightly more intense in fluorescence emissions, it appears that silica protects α-CDs from some quenching effect related to interactions with water.

The pH-monitoring tests with aqueous dispersions of silica−Cdots (initial pH of 4.30) were performed according to the setup shown in Figure 4A. Briefly, the dispersions had the pH

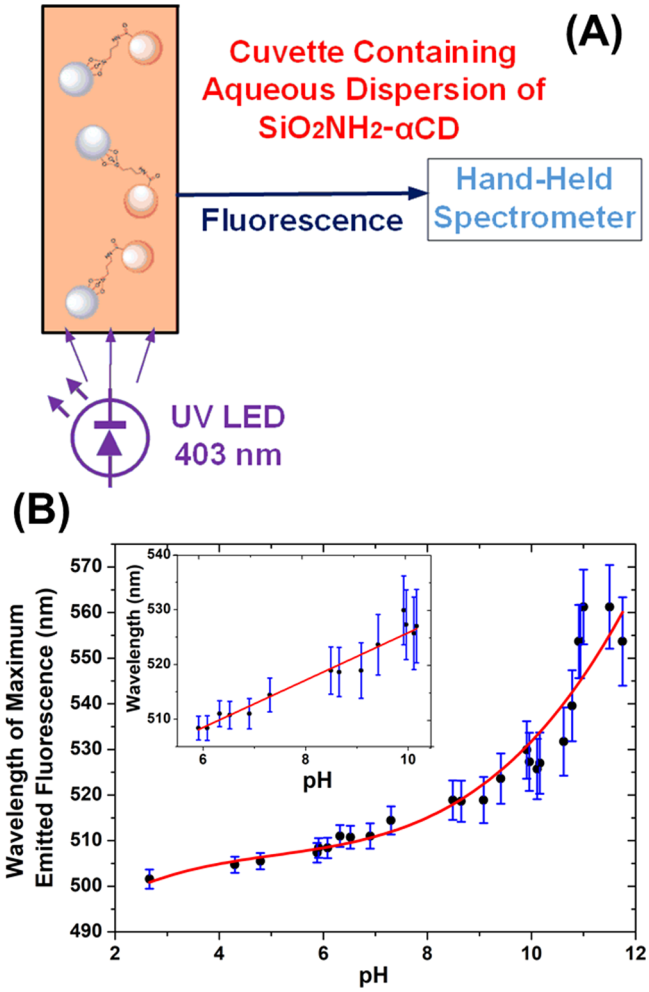

Figure 4. (A) Setup for the pH evaluation using the aqueous hybrids dispersions. (B) Wavelength of maximum emitted fluorescence as a function of pH for the dispersions of hybrids. The inset shows the linear portion of the curve (pH ranging from 6 to 10).

modified by first adding NaOH, and then the pH was reduced with HCl (both solutions 0.01 M). For each tested pH, the dispersions were introduced into cuvettes and were irradiated with a 403 nm LED to have the emission spectra analyzed. The wavelengths corresponding to the peaks of maximum emitted intensities were retrieved, and data were correlated to the pHs. Figure S15 shows photographs of one sample during the test and under daylight.

The results are shown in Figure 4B. They were fitted by a cubic polynomial relating the maximum wavelength to the pH (wavelength = 467.23 + 20.17(pH) − 3.45(pH)^2 + 0.20(pH)^3,

https://doi.org/10.1021/acsanm.1c02127
ACS Appl. Nano Mater. 2021, 4, 9738−9751

adjusted R^2 = 0.91), proving that it is possible to optically monitor the acidity. It is also interesting to note that the increase in pH leads to a red-shift of the emitted fluorescence. Besides that, the fluorescence is stable and reversible regarding the pH. Indeed, the wavelength of maximum emitted intensity easily returns to its previous value by simply reversing the pH change.

This red-shift verified when increasing the pH may be interpreted in terms of the interactions between the nanoparticles and the solvent, which results in modifications of the excited-state stability. According to Sciortino et al.,[52] CDs emission energies show a notable and systematic dependence on solvent characteristics, as well as a strong response of the photoexcited particles to the presence of hydrogen bonds. As a consequence, CDs may be used as solvent polarity nanoprobes to monitor neighboring ions and molecules. The authors verified that the CDs' emission blue-shifts as the solvent polarity is reduced. The lowest wavelength was observed for water due to the stabilization effect of the hydrogen bonds. Their conclusion was that both the nitrogen and carboxylic acid groups that may be present on the CDs' surfaces act as efficient hydrogen-bond acceptors. This is due to their electron lone pairs, and thus, the fluorescence mechanism is closely related to the presence of these groups on the subnanometric surface shell around the carbon nuclei.[52] In turn, Bano et al.[53] used latex as the raw material for the production of CDs containing carboxylic acid groups on their surfaces. They verified that the increase in the medium's acidity led to the protonation of the carboxylic surface groups of the dots. Consequently, the particles' negative charges decreased (or were even neutralized) in lower pHs, and the colloidal dispersions lost stability. This ultimately resulted in the aggregation of the CDs and in the extinction of the fluorescence.[53] A similar effect was observed by Chandra et al.,[54] but it was analyzed in terms of the UV−vis absorbance spectrum: in basic media, the deprotonation of the surface acid groups of CDs caused an intense decrease in the radiation absorption.

In our case, the silica−Cdots present chemical and structural differences compared to the α-CDs, which may impact their interactions with the solvent. The most important ones are the slightly superior dimensions of the particles (which affects the sizes of the dynamic cavities/first solvent shells[55,56]) and the fact that there may be fewer carboxylic groups, since −COOH reacts with a-SiO_2. On the other hand, Scheme 1 shows the presence of other lone pairs on the hybrid surfaces. There are lone pairs from the amide group (the bond between SiO_2 and α-CD), the Si−O− bonds between silica and α-CD, and other −Si−OH and −Si−O−O−Si− groups that may exist, since these defects are commonly observed on SiO_2 surfaces.[47,48]

Therefore, the surface groups of the silica−Cdots hybrids selectively detect Na^+ or Cl^- ions present in the controlled pH solutions. The main chemical groups of the hybrids, identified by XPS, are the COOH of the carbon nanodots (α-CDs), the NH−(C═O) from the amide group (the bond between SiO_2 and α-CD), the Si−O− bonds between silica and α-CD, and other −Si−OH and −Si−O−Si− groups and Si−O. The wavelength of the fluorescence emitted from the hybrids, measured at the highest emission intensity, is selectively shifted and quenched because of the interactions among the hybrids' surface groups and ions in the aqueous solution.

At this moment, considering that the pH of the initial aqueous solution is clearly acidic (4.30) and that there are still several groups capable of hydrogen bonding (stabilizing the excited states), we can consider that the hybrids behave as the other acidic carbon nanodots cited.[52−54] Therefore, analogous conclusions can be made for the results of wavelength shifts with the pH depicted in Figure 4: as the pH gets more basic, the deprotonation of the carboxylic groups of the hybrids' surfaces increases their negative charges and, consequently, enhances the hydrogen-bond interactions between the particles and the solvent (water). Since this effect causes the stabilization of the fluorophores, the red-shift is observed.[35,52] The possibly lower number of −COOH groups is not necessarily a problem here: it is known that basic pHs (higher than 10) usually deprotonate colloidal and nanostructured silica's silanol groups,[47,57,58] increasing the hybrids' charges.

The inset of Figure 4 shows a portion of the curve between pHs 6 and 10, which can be fitted by a linear polynomial (wavelength = 480.95 + 4.53(pH), adjusted R^2 = 0.95). Once this is the region of maximum variation of wavelength with pH, the derivative of this linear portion allows the calculus of the sensitivity (i.e., the rate of variation of the signal in relation to the measured parameter[18]) of the liquid phase silica−Cdots dispersions for the detection of pH changes: 4.53 nm/(pH unit).

Moreover, one can notice that, as the pH gets closer to 2, the curve reaches a signal baseline. It leads to a drop in sensitivity and makes it difficult to perform readings for more acidic media. As the pH is raised to 12, in turn, one can observe an increase in both the noise of the observed fluorescence spectra and the dispersion of data in Figure 4B. However, this is not an issue for industrial purposes. That is because only the use of the linear range with highest sensitivity is indicated for these situations, since it facilitates the design of the automation system.[42,59] Therefore, considering these results, we decided not to test pHs lower than 2 or higher than 12 for the agar waveguide doped with hybrids.

pH Sensing with the Agar Waveguide. Once the possibility of using the hybrids as pH nanoprobes in water was verified, the nanoparticles were used for the fabrication of a biodegradable and biocompatible pH-sensing device. For this purpose, silica−Cdots (3.10 g/L) and agarose (30.0 g/L) were mixed in DI water, heated close to the boiling point, and introduced into cylindrical molds for curing at ∼10 °C. A fluorescent agar waveguide was then obtained (Scheme 2). Also, an agar cylinder containing no hybrids was simultaneously fabricated under the same conditions and used for comparison.

The light transmission spectra of both the doped waveguide and of the agar containing no nanoparticles were obtained by transmitting a supercontinuum laser through the materials (Figure 5A). For comparison, the spectrum of the light source is presented in Figure S16. Finally, the same test performed for the aqueous dispersions was repeated for the doped waveguide (correlation of the wavelength of the peak of maximum fluorescence intensity with the pH, when the sample is excited by a 403 nm LED). These results are shown in Figure 5B. The photographs obtained for the waveguides under daylight and when transmitting the supercontinuum laser are shown in Figure S17. This last figure shows that the occlusion of the hybrids gives a brown/orange color to the waveguides and reduces their transparency to the visible.

Before analyzing the results of Figure 5, it is interesting to discuss the selection of this particular concentration of hybrids (3.10 g/L of hybrids in aqueous solution with 30.0 g/L of agarose). In fact, different proportions of silica−Cdots, agarose, and water were tested.

Since the NA increases with the polymer's refractive index (eq S1), enhancing the light-guiding efficiency, the first tests

https://doi.org/10.1021/acsanm.1c02127
ACS Appl. Nano Mater. 2021, 4, 9738−9751

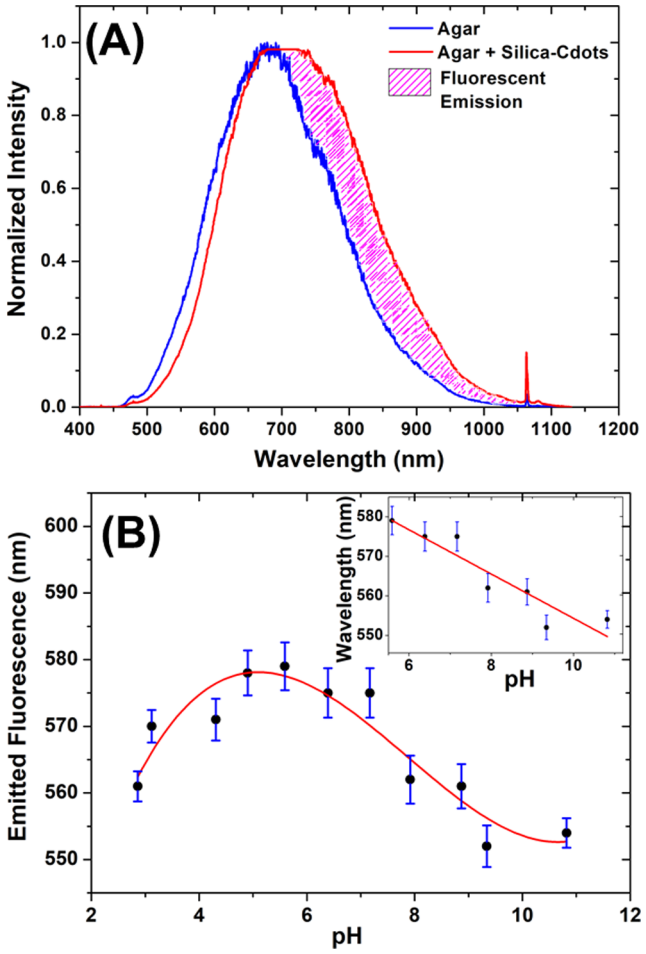

Figure 5. (A) Intensity of light transmitted by the waveguides (excitation with the supercontinuum laser). The dashed region corresponds to the fluorescence of the hybrids. (B) Wavelength of maximum emitted fluorescence as a function of pH for the agar waveguide. The inset shows the linear portion of the curve (pH 6−10).

consisted in evaluating whether the agar concentration significantly changed the RI of the mother liquor. Thus, the refractive indexes of solutions containing different concentrations of agar in DI water were collected. These results are shown and extensively discussed in the Supporting Information (Figure S18). Briefly, very low variations (on the order of only 10^{-4} refractive index units, RIU) were observed when increasing the agar concentration. In addition, the RI of the precursor solutions was not higher than 1.3334, which is very close to the water's RI (1.3330). Then, the amount chosen for the fabrication of the doped cylinder (30 mg of agar/mL of water) was the one that not only resulted in the higher RI but also in a waveguide with mechanical consistency and with sufficient optical transparency. Another requirement was that, after being doped, the waveguide should allow both the stimulation of the hybrids by the external source and the further collection of the fluorescence. However, there is a commitment to the presence of the nanoparticles that severely increases the opacity of the waveguides because of additional mechanisms of absorption and scattering of the light. We verified that, if agar concentrations higher than 30.0 g/L were used, there was sufficient transparency only when working with low concentrations of hybrids. These low concentrations, in turn, resulted in low luminescence and difficulty of detection.

The selection of the silica−Cdots concentration was analogous: 3.10 g/L (∼10% m/v) was the value that resulted in the highest luminescence signal. Increasing the concentration even more would lead to a result opposite to the desired: the device would get so opaque that no luminescence could be observed. Then, light sources with much higher power would be required. Since this would also impact the selection of the excitation wavelength, as discussed in the Supporting Information, we decided to apply the concentration of 3.10 g/L. Finally, as mentioned in the Experimental Section, the solution of eq S1 resulted in a high NA (0.882) for the RI of the doped agar after curing (RI = 1.3334, air-cladding), and Figure S17F indeed shows there is excitation and guiding of the luminescence.

The intensities of light transmitted by the net agar and the silica−Cdots doped agar waveguides as a function of wavelength are shown in Figure 5, parts A and B, respectively. The light intensities were obtained after exciting the waveguides with a supercontinuum laser, and then collecting the transmitted light at the end-face (Scheme 2, Figure S17, parts C and F).

When comparing the transmission profile obtained for the agar containing no nanoparticles with the spectrum of the source (shown separately in Figure S16), one can notice they present essentially the same format, with almost no attenuation. It could be concluded that there is no emission in this situation (as expected, since no fluorescent particles were added). Besides, the interaction between the polymer and the light does not appear to broaden or to distort the transmission profile. That is not the case for the doped agar. First, the maximum intensity appears to be shifted from 680 nm (the wavelength of maximum intensity emitted by the source, as shown in Figure S16) to 705 nm.

It is also possible to notice that, until ∼700 nm, the doped-agar waveguide (red curve of Figure 5A) follows approximately the same pattern as the light source, but with attenuated intensity when compared to the material containing only agar (blue curve of Figure 5A). This was already expected from the increased opacity. Then, after 700 nm, the curve for the doped waveguide overcomes the agar curve, as evidenced by the pink dashed region of Figure 5A. From 700 nm, the light spectrum collected at the end-face of the waveguide doped with silica−Cdots is clearly broader and more intense than both the spectra transmitted by the device containing only agar and by the supercontinuum laser (Figure S16).

On the other hand, Figure 3B already showed that excitations higher than 400 nm resulted in fluorescence emissions extending over 700 nm for the particles dispersed in water, and shifts of the spectra are expected when modifying the medium from water to agar. If the excited particles were better stabilized in the new medium, then the red-shift of the spectra would result in emissions at even higher wavelengths.[35,52−56] Moreover, the intensity profile collected at the end-face of the waveguide is actually a result from the combination of the luminescence with the light interactions with all the chemical species present in the system.[18,35,60,61]

Therefore, we can conclude that the occlusion of silica−Cdots in the polymeric matrix modifies the agarose's transmission profile. Additionally, the new spectrum is broader and more intense after 700 nm, which results from the balance between the light source excitation, the fluorescence emitted by the nanohybrids, and the absorption, scattering, and other attenuation mechanisms by the polymer, adsorbed water molecules, and hybrids themselves.[18,35,61]

https://doi.org/10.1021/acsanm.1c02127
ACS Appl. Nano Mater. 2021, 4, 9738−9751

After the visible light transmission characterization (Figure 5A), the waveguides were submitted to preliminary tests with the 403 nm LED, the same source used for pH detection in the aqueous phase (previously discussed in Figure 4). In these tests, the doped waveguides were irradiated by the LED in one of their ends, and light emerging from the waveguides was collected in two different positions: from the end-face and from the sidewalls of the waveguides (agar cylinders). As expected, the luminescent emission was observed. It was also verified that the different light collection positions caused no significant modifications in the wavelengths, corresponding to the peaks of maximum luminous intensity. Therefore, the configuration that maximized the detected intensity, i.e., the setup with light collected at the end-face (Scheme 2), was chosen for the tests. The luminous intensities were collected with the spectrometer, and then were normalized for retrieving the wavelength information corresponding to each pH (wavelength interrogation-based sensing). Finally, it is important to mention that different lengths of agarose-doped cylinders (from 1 to ∼7 cm long) were tested. We verified that the chosen LED power and precursor concentrations allowed us to perform the analyses for all of these lengths, despite of the increasing attenuation.

Due to the satisfactory preliminary results obtained when using visible light and the 403 nm LED, the waveguides were immersed in DI water until getting again fully swollen. When this condition was reached, there was no more visible variation of their diameters and the pH reading corresponding to the aqueous phase got stabilized, indicating that the materials could be applied to the pH sensing tests.

As discussed, before the first addition of NaOH, the pH of the dispersion of hybrids in DI water was acidic (4.30) because of the presence of the carboxylic groups (Figure 4). The pH of the DI water used to keep the doped waveguides swollen (i.e., the water maintained in equilibrium with the waveguides, prior to the sensing tests), in its turn, is less acidic (pH = 5.59). The agarose molecular structure does not contain groups that directly change the pH (only C−OH and C−O−C groups);[36] thus, this pH variation was not expected from the polymer's chemical structure. It is probably a consequence of the lower concentration of hybrids used for the fabrication of a waveguide with suitable transparency (3.10 g/L) and of the influence of the hydrogel matrix on the acidic equilibrium of the nanohybrids. Since this equilibrium analysis is beyond the scope of this study (which aimed to fabricate and to test the performance of the waveguide on the pH assessment), this investigation was left for future research.

Since both the agarose and the hybrids are very hygroscopic, the waveguides' intumescence degree and the aqueous phase pH readings take no longer than 30 s to stabilize when base or acid are added. Thus, the waveguides were kept immersed and under stirring (25 °C) to ensure the homogeneity of the aqueous medium. Again, the pH was first raised to ∼12 (addition of 0.01 M NaOH), and then reduced to ∼2 (dropping of 0.01 M HCl). When the pH reading got stable after a given addition of NaOH or HCl, the waveguide was rapidly excited with the LED to have its fluorescence spectrum collected (as in Scheme 2).

It is important to mention that the wavelength interrogation is independent from the total amount of fluorophores, an important advantage of this approach compared to intensity-based sensing techniques.[5,18,61] Therefore, since the signals obtained for all of the tested pH ranges (Figure 4B and Figure 5B) were sufficient for retrieving the wavelength of the peaks of maximum fluorescence, it was not necessary to correlate the measurements with the added volume. The evaluation of quenching mechanisms due to the presence of metal ions[61] was also beyond the scope of this study. Thus, as all the tested media allowed the data collection, different concentrations of cations were not deliberately added. All of the experiments shown in Figure 5B were conducted under the same temperature and atmospheric air conditions. Then, the modifications of the spectra could be correlated to the changes in solvent polarity, as in the other mentioned reports.[35,52−56]

Interesting conclusions are also obtained when comparing, for a same pH, the fluorescence spectrum collected for the doped waveguide with the one obtained for the aqueous dispersion of silica−Cdots (i.e., when comparing the spectra used for obtaining the information in Figure 5B and Figure 4B). An example of the general observed behavior is shown in Figure S19, where the spectra collected for pH 4.30 are compared (both systems excited by the 403 nm LED).

Figure S19 shows that the peak (maximum intensity of fluorescence) of the hybrids occluded into the hydrogel matrix is red-shifted compared to the one observed for the aqueous dispersion of silica−Cdots. This indicates an increase in the stability of the excited states,[21,35,61] and this same shift was observed for all the other pHs. It is also possible to verify in Figure S19 that the signals collected for the doped waveguide present higher noise (here, the noise is taken as the difference between the signals and the average fitted curves of the figure).[18]

The solvatochromic shifts resulting from the enclosure of fluorescent species into rigid media are complex phenomena, as extensively discussed by other researchers.[21,35,52−56,61] The observed shifts depend, for example, on the method used for preparing the matrix and on the particular technique applied to the incorporation of the fluorophores.[21] For soluble polymers, in particular, an increase in the medium's polarity or in the intensity of the solute−matrix hydrogen-bond interactions may result in the reduction of the energy difference between the ground and the excited states, red-shifting the emission.[21,35,52]

Thus, the red-shift observed in Figure S19 may be explained analogously as performed by other authors who analyzed the increase in the nanoparticles' excited-state stability when the CDs are incorporated into hydrogel matrixes with plenty of oxygen and hydroxyl groups. For PVA, for example, the matrix networks form many hydrogen bonds with the polar groups of CDs, stabilizing the emissive states.[35] This same phenomenon is expected to take place between the agarose's C−OH and C−O−C groups[37] and the silica−Cdots' oxygen and nitrogen groups (Figure 2). According to Jiang et al.,[35] in some hydrogels, these interactions may be so intense that they even result in composites showing phosphorescence or delayed fluorescence.

Figure 5B summarizes the correlation between the wavelengths of the maximum emitted intensity (the peaks) and the pHs of the aqueous media where the doped waveguides were immersed. Contrary to what was observed for the aqueous dispersions (Figure 4B), the agar waveguides show a critical point for the results, which is again probably due to the interactions between the hybrids and the hydrogel matrix.[35,36] The critical point corresponds to the initial situation: it is the pH (5.59) of the water initially in equilibrium with the agar, which was used to keep the device swollen before adding NaOH or HCl.

Once the wavelength of the maximum fluorescence emitted as a function of pH has been obtained (Figure 5B), by first raising, and then reducing, the pH, it is shown that the wavelengths of

https://doi.org/10.1021/acsanm.1c02127
ACS Appl. Nano Mater. 2021, 4, 9738−9751

maximum intensity present reversibility regarding pH: they easily return to previous values after HCl addition.

The results were also quite repeatable. Again, they were fitted by a third-degree polynomial correlating the maximum wavelength to the pH, given by wavelength = 474.21 + 48.50(pH) − 7.03(pH)^2 + 0.30(pH)^3, adjusted R^2 = 0.83. Despite the fact that no clear baseline was reached, the light intensity signals suffer substantial decreases as the pH gets closer to 2 or 12, indicating that the sensor is not adequate for monitoring pHs beyond these values.

This pH range (2−12), however, is wider than the one obtained by Zhang et al.[38] (pHs from 2 to 7). It is also wider than the range achieved by Chen et al.:[41] as mentioned, they obtained a system able to detect pHs from 3.0 to 11.0, but using a more complicated sensing strategy (ratiometric analysis). In their study, dispersions combining CdTe QDs and CDs in an aqueous phase and under different pHs were introduced into a fluorometer, where the data were collected. Each tested pH resulted in two different curves correlating the emitted intensity to the emission wavelength, one for the QDs and the other for the CDs. The two peaks of maximum intensity were obtained by the fluorometer, and the ratio between them was calculated. Finally, a calibration curve related this peak ratio to the pH.[41]

As in Figure 4B, Figure 5B shows a linear portion with maximum rate of variation (inset of Figure 5B). This region corresponds to the pH range from 6 to 10 and may be fitted by a first-degree polynomial (wavelength = 610.35 − 5.61(pH), adjusted R^2 = 0.84). The derivative of this polynomial is negative, contrary to that observed for the aqueous dispersions (inset of Figure 4B). The modulus of the derivative was taken as the sensitivity[18] of the silica−Cdots/agarose sensor in relation to the pH, and it was calculated as 5.61 nm/(pH unit).

It is interesting to notice that the applied setup (Scheme 2) could be easily adapted to perform the online evaluation of the pH directly in the liquid medium. This would be done by transporting the light with external optical fibers (like in Choi et al.[9]): one fiber would guide the light from the LED to one extremity of the agar waveguide, and a second one would collect it at the end-face and guide it to the optical analyzer.

The clear drawback is that this adaptation would result in the lowering of the NA and of the guiding efficiency: as shown in the Supporting Information, NA decreases to 0.054 in water (eq S1). On the other hand, the small lengths of agarose waveguides used in this study (up to ∼70 mm) lead to low power losses, as discussed when analyzing Figure 5A. Then, the reduced NA is not expected to be an impeditive factor to this setup modification.[18]

However, we chose not to proceed with this adaptation because it would not allow the evaluation of the sensor capability in retaining information even when it is removed from the assessed medium. This last analysis is particularly important, since there are several practical applications where a waveguide capable of retaining the medium information is required.

In a biomedical environment, for example, it may be necessary to remove the sensor from the medium to analyze other parameters besides pH. This situation has been reported and analyzed in studies where hydrogel matrixes are simultaneously used as waveguides and as scaffolds for growing cells,[7,9] with the need for cell counting. In the standard counting procedure, samples are periodically collected from the analyzed biosystem to be observed and counted on the microscope using specific devices, such as the Neubauer chamber.[62] If the waveguides can be removed and their volumes are known, the chamber may be substituted by the waveguide itself. Then, the cellular environment is not disturbed, reducing the risk of causing cell death during counting.[7,9]

As Figure 5B and Figure S17 show, the pH information is actually retrieved by the silica−Cdots/agarose waveguide when it is removed from the aqueous medium. Therefore, since the waveguide can be removed and analyzed off-line, this novel device has potential for monitoring other important biochemical parameters in addition to pH (e.g., the number of cells, previously cited, or the morphological characteristics of the doped agar).

A final important comparison to be performed is with commercial pH meters. As mentioned, we noticed a decrease of the detected fluorescence intensity as the pHs got closer to 12, preventing the detection beyond this condition.

However, many commercial pH meters also show loss of signal intensity or difficulties in evaluating very alkaline media. Indeed, it is widely known that the traditional devices may lose precision when submitted to such conditions.[60,63−65] That is because these devices commonly show substantial interference caused by the presence of Na^+ ions when under pHs > 12 (they interpret Na^+ as H^+ ions).[60,63] As a solution to this problem, many manufacturers provide tables correlating the detected pH to the ionic concentrations and estimating reading corrections,[63] or they indicate devices specifically designed for higher pH ranges or more drastic operational conditions.[63−65]

Lastly, the recovery of fluorescent silica−Cdots hybrids embedded into the agarose, after being discarded, is technically feasible. Since the agarose is biodegradable, it can be solubilized in water and the hybrids separated by centrifugation. It would be interesting to carry out a study to verify the technical−economic feasibility in the recovery of hybrids, considering that they are low-cost and environmentally friendly materials.

CONCLUSIONS

In summary, we reported an efficient methodology for the fabrication of biodegradable, biocompatible, and fluorescent cylindrical waveguides doped with hybrid amorphous nanoparticles (silica−Cdots). The fluorescence spectra of the amorphous α-CDs and of the hybrids dispersed in water were analyzed, and it was verified that the coupling caused a red-shift of the wavelength corresponding to the maximum emitted intensity. The hybrids are easier to handle than no-coupled carbon nanodots, since they are less hygroscopic. Therefore, they are more adequate for the fabrication of large volumes of agarose waveguides.

The aqueous dispersion of silica−Cdots showed sensitivity regarding the pH, 4.53 nm/(pH unit). Then, agarose was doped with these particles for the fabrication of the pH sensor. The obtained hydrogel-based waveguide showed stable and reversible behavior regarding pH and a maximum sensitivity of 5.61 nm/(pH unit) when excited by a 403 nm UV LED (sensitivity calculated for the pH range of 6−11). Since the pH information is retrieved when the waveguide is removed from the aqueous medium, the system offers a low-cost, disposable, and simplified pH sensor that can be used in multiparameter biomedical analysis. Moreover, commercial pH meter membranes present the practical disadvantage of being commonly made of highly fragile glass.[60,63−65]

In fact, there are already crystal and polymer pH meter membranes available, but most of the commercial electrodes used in general applications (including biological, pharmaceutical, and petroleum emulsions applications) still rely on glass

https://doi.org/10.1021/acsanm.1c02127
ACS Appl. Nano Mater. 2021, 4, 9738−9751

membranes. These membranes, in turn, must be maintained under strict temperature conditions and have to be stored immersed in appropriate saline solution, usually 3 M KCl in water.[63−65] Since the proposed sensor is made of an elastomeric material (the hydrogel), it presents higher tenacity than the commercial glass devices, with lower risks of mechanical fracture.[3,36,60]

The verification of the solvatochromic shifts related to pH variations and to the occlusion of the silica−Cdots into agarose is also of particular importance. That is because these data provide insights regarding the interaction mechanisms between fluorescent nanoparticles and their media. As mentioned by Sciortino et al.,[52] there is still a lack of research analyzing (or even verifying) the effects of the incorporation of carbon nanodots into different solid media on the luminescence emissive mechanisms.

Finally, the synthesized amorphous hybrids could also be very interesting as new materials for applications in optoelectronic devices, optical fibers sensors, and solar cells. Forthcoming studies will exploit the direct coupling between carboxylic acid terminated carbon nanodots and the amino-functionalized silica surface of no-core optical fibers (basically, a silica cylinder) for the fabrication of a fluorescent cladding with sensing applications in media of different polarities.

■ ASSOCIATED CONTENT

Supporting Information

The Supporting Information is available free of charge at https://pubs.acs.org/doi/10.1021/acsanm.1c02127.

Visual comparison between particles, selection of the light source for the pH sensing tests (403 nm LED), numerical aperture evaluation, α-CDs UV−vis absorbance, TEM and FEG-TEM images of particles, comparison between the FT-IR spectra of the particles, TGA and XPS and XRD analyses of the particles, Raman spectra of the particles, setup for pH evaluation in the aqueous phase, emission spectrum of the light source (supercontinuum laser), agar and silica−Cdots doped waveguides under daylight and supercontinuum, RI of the waveguide as a function of the agar concentration, and emission spectra of silica−Cdots under 403 nm and pH 4.30 (water and agar) (PDF)

■ AUTHOR INFORMATION

Corresponding Authors

Julio Roberto Bartoli − *School of Mechanical Engineering, State University of Campinas, Campinas, São Paulo, Brazil 13083-860; Laboratory of Dielectrics, Optical and Nanocomposites Materials, Department of Materials and Bioprocess Engineering, School of Chemical Engineering, State University of Campinas, Campinas, São Paulo, Brazil 13083-852;* orcid.org/0000-0002-7946-8962; Email: bartoli@unicamp.br

Maurizio Prato − *Department of Chemical and Pharmaceutical Sciences, University of Trieste, 34127 Trieste, Italy; Center for Cooperative Research in Biomaterials, Basque Research and Technology Alliance, 20014 Donostia San Sebastián, Spain; Basque Foundation for Science, Ikerbasque, 48013 Bilbao, Spain;* orcid.org/0000-0002-8869-8612; Email: prato@units.it

Authors

Francesco Amato − *Department of Chemical and Pharmaceutical Sciences, University of Trieste, 34127 Trieste, Italy*

Marco César Prado Soares − *School of Mechanical Engineering, State University of Campinas, Campinas, São Paulo, Brazil 13083-860; Gleb Wataghin Institute of Physics, State University of Campinas, Campinas, São Paulo, Brazil 13083-859;* orcid.org/0000-0002-5219-5124

Thiago Destri Cabral − *School of Mechanical Engineering, State University of Campinas, Campinas, São Paulo, Brazil 13083-860; Gleb Wataghin Institute of Physics, State University of Campinas, Campinas, São Paulo, Brazil 13083-859*

Eric Fujiwara − *School of Mechanical Engineering, State University of Campinas, Campinas, São Paulo, Brazil 13083-860*

Cristiano Monteiro de Barros Cordeiro − *Gleb Wataghin Institute of Physics, State University of Campinas, Campinas, São Paulo, Brazil 13083-859;* orcid.org/0000-0002-8787-0636

Alejandro Criado − *Center for Cooperative Research in Biomaterials, Basque Research and Technology Alliance, 20014 Donostia San Sebastián, Spain*

Complete contact information is available at: https://pubs.acs.org/10.1021/acsanm.1c02127

Author Contributions

All authors have given approval to the final version of the manuscript.

Notes

The authors declare no competing financial interest.

■ ACKNOWLEDGMENTS

The authors thank the São Paulo Research Foundation (FAPESP, Brazil) under Grant 2019/22554-4, the National Council for Scientific and Technological Development (CNPq, Brazil) (Finance Code −001), Espaço da Escrita—Pró-Reitoria de Pesquisa—UNICAMP for the language services provided and Faepex/Unicamp, M. Möller (CIC biomaGUNE-BRTA) for the FEG-TEM analysis, Professor S. Bosi, Dr. F. Arcudi, Dr. G. Filippini, Dr. M. Cacioppo (DSCF/UNITS), Dr. P. Bertoncin (DSV/UNITS), Professor C. K. Suzuki (FEM/Unicamp), Professor M. Carreño, and Professor I. Pereyra (LME/EPUSP) for the technical support and for scientific discussions and insights, and Gildo S. Rodrigues (Unicamp) for the 3D printing of the molds. Professor Maurizio Prato is the AXA Chair for Bionanotechnology (2016−2023). This study was supported by the University of Trieste, INSTM, the Italian Ministry of Education, MIUR (cofin Prot. 2017PBXPN4), and the Spanish Ministry of Science, Innovation and Universities, MICIU (project PID2019-108523RB-I00). Part of this research was performed under the Maria de Maeztu Units of Excellence Program from the Spanish State Research Agency, Grant No. MDM-2017-0720.

■ REFERENCES

(1) Elsherif, M.; Moreddu, R.; Hassan, M. U.; Yetisen, A. K.; Butt, H. Real-Time Optical Fiber Sensors Based on Light Diffusing Microlens Arrays. *Lab Chip* **2019**, *19* (12), 2060−2070.

(2) Oliverio, M.; Perotto, S.; Messina, G. C.; Lovato, L.; De Angelis, F. Chemical Functionalization of Plasmonic Surface Biosensors: A

Tutorial Review on Issues, Strategies, and Costs. *ACS Appl. Mater. Interfaces* **2017**, *9* (35), 29394−29411.
(3) Omenetto, F. G.; Kaplan, D. L. A New Route for Silk. *Nat. Photonics* **2008**, *2* (11), 641−643.
(4) Cennamo, N.; Chiavaioli, F.; Trono, C.; Tombelli, S.; Giannetti, A.; Baldini, F.; Zeni, L. A Complete Optical Sensor System Based on a POF-SPR Platform and a Thermo-Stabilized Flow Cell for Biochemical Applications. *Sensors* **2016**, *16* (2), 196.
(5) Wolfbeis, O. S. Fiber-Optic Chemical Sensors and Biosensors. *Anal. Chem.* **2008**, *80* (12), 4269−4283.
(6) Jiang, N.; Ahmed, R.; Rifat, A. A.; Guo, J.; Yin, Y.; Montelongo, Y.; Butt, H.; Yetisen, A. K. Functionalized Flexible Soft Polymer Optical Fibers for Laser Photomedicine. *Adv. Opt. Mater.* **2018**, *6* (3), 1701118.
(7) Choi, M.; Humar, M.; Kim, S.; Yun, S. H. Step-Index Optical Fiber Made of Biocompatible Hydrogels. *Adv. Mater.* **2015**, *27* (27), 4081−4086.
(8) Zhou, M.; Guo, J.; Yang, C. Ratiometric Fluorescence Sensor for Fe^{3+} Ions Detection Based on Quantum Dot-Doped Hydrogel Optical Fiber. *Sens. Actuators, B* **2018**, *264*, 52−58.
(9) Choi, M.; Choi, J. W.; Kim, S.; Nizamoglu, S.; Hahn, S. K.; Yun, S. H. Light-Guiding Hydrogels for Cell-Based Sensing and Optogenetic Synthesis in Vivo. *Nat. Photonics* **2013**, *7* (12), 987−994.
(10) Đorđević, L.; Arcudi, F.; D'Urso, A.; Cacioppo, M.; Micali, N.; Bürgi, T.; Purrello, R.; Prato, M. Design Principles of Chiral Carbon Nanodots Help Convey Chirality from Molecular to Nanoscale Level. *Nat. Commun.* **2018**, *9* (1), 3442.
(11) Arcudi, F.; Đorđević, L.; Prato, M. Rationally Designed Carbon Nanodots towards Pure White-Light Emission. *Angew. Chem., Int. Ed.* **2017**, *56* (15), 4170−4173.
(12) Sun, Y.; Zhou, B.; Lin, Y.; Wang, W.; Fernando, K. A. S.; Pathak, P.; Meziani, M. J.; Harruff, B. A.; Wang, X.; Wang, H.; Luo, P. G.; Yang, H.; Kose, M. E.; Chen, B.; Veca, L. M.; Xie, S. Quantum-Sized Carbon Dots for Bright and Colorful Photoluminescence. *J. Am. Chem. Soc.* **2006**, *128* (24), 7756−7757.
(13) Yuan, F.; Li, S.; Fan, Z.; Meng, X.; Fan, L.; Yang, S. Shining Carbon Dots: Synthesis and Biomedical and Optoelectronic Applications. *Nano Today* **2016**, *11* (5), 565−586.
(14) Wang, Y.; Hu, A. Carbon Quantum Dots: Synthesis, Properties and Applications. *J. Mater. Chem. C* **2014**, *2* (34), 6921−6939.
(15) Huang, X.; Zhang, F.; Zhu, L.; Choi, K. Y.; Guo, N.; Guo, J.; Tackett, K.; Anilkumar, P.; Liu, G.; Quan, Q.; Choi, H. S.; Niu, G.; Sun, Y.-P.; Lee, S.; Chen, X. Effect of Injection Routes on the Biodistribution, Clearance, and Tumor Uptake of Carbon Dots. *ACS Nano* **2013**, *7* (7), 5684−5693.
(16) Arcudi, F.; Đorđević, L.; Prato, M. Synthesis, Separation, and Characterization of Small and Highly Fluorescent Nitrogen-Doped Carbon NanoDots. *Angew. Chem., Int. Ed.* **2016**, *55* (6), 2107−2112.
(17) Wang, X.; Qu, K.; Xu, B.; Ren, J.; Qu, X. Microwave Assisted One-Step Green Synthesis of Cell-Permeable Multicolor Photoluminescent Carbon Dots without Surface Passivation Reagents. *J. Mater. Chem.* **2011**, *21* (8), 2445.
(18) Saleh, B. E. A.; Teich, M. C. *Fundamentals of Photonics*; Wiley Series in Pure and Applied Optics; Goodman, J. W., Ed.; John Wiley & Sons, Inc.: New York, 1991.
(19) Pan, D.; Guo, L.; Zhang, J.; Xi, C.; Xue, Q.; Huang, H.; Li, J.; Zhang, Z.; Yu, W.; Chen, Z.; Li, Z.; Wu, M. Cutting Sp2 Clusters in Graphene Sheets into Colloidal Graphene Quantum Dots with Strong Green Fluorescence. *J. Mater. Chem.* **2012**, *22* (8), 3314.
(20) Zhu, S.; Zhang, J.; Qiao, C.; Tang, S.; Li, Y.; Yuan, W.; Li, B.; Tian, L.; Liu, F.; Hu, R.; Gao, H.; Wei, H.; Zhang, H.; Sun, H.; Yang, B. Strongly Green-Photoluminescent Graphene Quantum Dots for Bioimaging Applications. *Chem. Commun.* **2011**, *47* (24), 6858.
(21) Suppan, P. Invited Review Solvatochromic Shifts: The Influence of the Medium on the Energy of Electronic States. *J. Photochem. Photobiol., A* **1990**, *50* (3), 293−330.
(22) Filippini, G.; Amato, F.; Rosso, C.; Ragazzon, G.; Vega-Peñaloza, A.; Companyó, X.; Dell'Amico, L.; Bonchio, M.; Prato, M. Mapping the Surface Groups of Amine-Rich Carbon Dots Enables Covalent Catalysis in Aqueous Media. *Chem.* **2020**, *6* (11), 3022−3037.
(23) Choi, Y.; Jo, S.; Chae, A.; Kim, Y. K.; Park, J. E.; Lim, D.; Park, S. Y.; In, I. Simple Microwave-Assisted Synthesis of Amphiphilic Carbon Quantum Dots from A 3 /B 2 Polyamidation Monomer Set. *ACS Appl. Mater. Interfaces* **2017**, *9* (33), 27883−27893.
(24) Gong, X.; Ma, W.; Li, Y.; Zhong, L.; Li, W.; Zhao, X. Fabrication of High-Performance Luminescent Solar Concentrators Using N-Doped Carbon Dots/PMMA Mixed Matrix Slab. *Org. Electron.* **2018**, *63*, 237−243.
(25) Amato, F.; Cacioppo, M.; Arcudi, F.; Prato, M.; Mituo, M.; Fernandes, E.; Carreño, M.; Pereyra, I.; Bartoli, J. Nitrogen-Doped Carbon Nanodots/PMMA Nanocomposites for Solar Cells Applications. *Chem. Eng. Trans.* **2019**, *74*, 1105−1110.
(26) Đorđević, L.; Arcudi, F.; Prato, M. Preparation, Functionalization and Characterization of Engineered Carbon Nanodots. *Nat. Protoc.* **2019**, *14* (10), 2931−2953.
(27) Arcudi, F.; Ďord'ević, L.; Prato, M. Design, Synthesis, and Functionalization Strategies of Tailored Carbon Nanodots. *Acc. Chem. Res.* **2019**, *52* (8), 2070−2079.
(28) Martindale, B. C. M.; Hutton, G. A. M.; Caputo, C. A.; Reisner, E. Solar Hydrogen Production Using Carbon Quantum Dots and a Molecular Nickel Catalyst. *J. Am. Chem. Soc.* **2015**, *137* (18), 6018−6025.
(29) Soares, M. C. P.; Perli, G.; Bartoli, J. R.; Bertuzzi, D. L.; Taketa, T. B.; Bataglioli, R. A.; Suzuki, C. K.; Ornelas, C.; Fujiwara, E. Fast Microwave-Assisted Synthesis of Green-Fluorescent Carbon Nanodots from Sugarcane Syrup. In *2019 SBFoton International Optics and Photonics Conference (SBFoton IOPC)*; IEEE: São Paulo, SP, Brazil, 2019.
(30) Boobalan, T.; Sethupathi, M.; Sengottuvelan, N.; Kumar, P.; Balaji, P.; Gulyás, B.; Padmanabhan, P.; Selvan, S. T.; Arun, A. Mushroom-Derived Carbon Dots for Toxic Metal Ion Detection and as Antibacterial and Anticancer Agents. *ACS Appl. Nano Mater.* **2020**, *3* (6), 5910−5919.
(31) Xu, Q.; Su, R.; Chen, Y.; Theruvakkattil Sreenivasan, S.; Li, N.; Zheng, X.; Zhu, J.; Pan, H.; Li, W.; Xu, C.; Xia, Z.; Dai, L. Metal Charge Transfer Doped Carbon Dots with Reversibly Switchable, Ultra-High Quantum Yield Photoluminescence. *ACS Appl. Nano Mater.* **2018**, *1* (4), 1886−1893.
(32) Xu, Q.; Li, W.; Ding, L.; Yang, W.; Xiao, H.; Ong, W. J. Function-Driven Engineering of 1D Carbon Nanotubes and 0D Carbon Dots: Mechanism, Properties and Applications. *Nanoscale* **2019**, *11* (4), 1475−1504.
(33) An, Y.; Chen, M.; Xue, Q.; Liu, W. Preparation and Self-Assembly of Carboxylic Acid-Functionalized Silica. *J. Colloid Interface Sci.* **2007**, *311* (2), 507−513.
(34) An, J.; Chen, R.; Chen, M.; Hu, Y.; Lyu, Y.; Liu, Y. An Ultrasensitive Turn-On Ratiometric Fluorescent Probes for Detection of Ag+ Based On Carbon Dots/SiO2 and Gold Nanoclusters. *Sens. Actuators, B* **2021**, *329*, 129097.
(35) Jiang, K.; Wang, Y.; Li, Z.; Lin, H. Afterglow of Carbon Dots: Mechanism, Strategy and Applications. *Mater. Chem. Front.* **2020**, *4* (2), 386−399.
(36) Burey, P.; Bhandari, B. R.; Howes, T.; Gidley, M. J. Hydrocolloid Gel Particles: Formation, Characterization, and Application. *Crit. Rev. Food Sci. Nutr.* **2008**, *48* (5), 361−377.
(37) Wang, L.; Li, M.; Li, W.; Han, Y.; Liu, Y.; Li, Z.; Zhang, B.; Pan, D. Rationally Designed Efficient Dual-Mode Colorimetric/Fluorescence Sensor Based on Carbon Dots for Detection of PH and Cu2+ Ions. *ACS Sustainable Chem. Eng.* **2018**, *6* (10), 12668−12674.
(38) Zhang, T.; Dong, S.; Zhao, F.; Deng, M.; Fu, Y.; Lü, C. Tricolor Emissive Carbon Dots for Ultra-Wide Range PH Test Papers and Bioimaging. *Sens. Actuators, B* **2019**, *298*, 126869.
(39) Soares, M. C. P.; Mendes, B. F.; Gomes, M. K.; Bataglioli, R. A.; Schenkel, E. A.; Vit, F. F.; de la Torre, L. G.; Fujiwara, E.; Suzuki, C. K. Optical Fiber Sensor as an Alternative for Colorimetric Image Processing for the Assessment of Dye Concentration. In *2018 SBFoton International Optics and Photonics Conference (SBFoton IOPC)*; IEEE: Campinas, SP, Brazil, 2018.

https://doi.org/10.1021/acsanm.1c02127
ACS Appl. Nano Mater. 2021, 4, 9738−9751

(40) Skibicki, J.; Golijanek-Jedrzejczyk, A.; Dzwonkowski, A. The Influence of Camera and Optical System Parameters on the Uncertainty of Object Location Measurement in Vision Systems. *Sensors* **2020**, *20* (18), 5433.
(41) Chen, Y.; Zhao, C.; Wang, Y.; Rao, H.; Lu, Z.; Lu, C.; Shan, Z.; Ren, B.; Wu, W.; Wang, X. Green and High-Yield Synthesis of Carbon Dots for Ratiometric Fluorescent Determination of PH and Enzyme Reactions. *Mater. Sci. Eng., C* **2020**, *117*, 111264.
(42) Bailey, J.; Ollis, D. *Biochemical Engineering Fundamentals*; McGraw-Hill: New York, 1986.
(43) *AEROSIL − Fumed Silica Technical Overview*. Evonik Industries, 2015. https://www.silica-specialist.com/product/aerosil/downloads/technical-overview-aerosil-fumed-silica-en.pdf (accessed 2021-07-17).
(44) Uchino, T.; Aboshi, A.; Kohara, S.; Ohishi, Y.; Sakashita, M.; Aoki, K. Microscopic Structure of Nanometer-Sized Silica Particles. *Phys. Rev. B: Condens. Matter Mater. Phys.* **2004**, *69* (15), 1−8.
(45) Silverstein, R. M.; Webster, F. X.; Kiemle, D. J. *Spectrometric Identification of Organic Compounds*, 7th ed.; John Wiley & Sons: New York, 2005; pp 72−126.
(46) Beganskienė, A.; Sirutkaitis, V.; Kurtinaitienė, M.; Juškėnas, R.; Kareiva, A. FTIR, TEM and NMR Iinvestigations of Stöber Silica Nanoparticles. *Mater. Sci.* **2004**, *10* (4), 287−290.
(47) Iler, R. K. *The Chemistry of Silica*; John Wiley and Sons: New York, 1979.
(48) Götze, J.; Möckel, R. *Quartz: Deposits, Mineralogy and Analytics*; Springer: Berlin Heidelberg, 2012.
(49) Casamassima, M.; Darque-Ceretti, E.; Delamare, F.; Aucouturier, M. C. R. Characterization by XPS of Electron Donor/Acceptor Properties of Aluminum and Silicon Oxide Surfaces. *C. R. Acad. Sci. Ser. II* **1991**, *313*, 25−30.
(50) Ederer, J.; Janoš, P.; Ecorchard, P.; Tolasz, J.; Štengl, V.; Beneš, H.; Perchacz, M.; Pop-Georgievski, O. Determination of Amino Groups on Functionalized Graphene Oxide for Polyurethane Nanomaterials: XPS Quantitation vs. Functional Speciation. *RSC Adv.* **2017**, *7* (21), 12464−12473.
(51) Tougaard, S. Improved XPS Analysis by Visual Inspection of the Survey Spectrum. *Surf. Interface Anal.* **2018**, *50* (6), 657−666.
(52) Sciortino, A.; Marino, E.; van Dam, B.; Schall, P.; Cannas, M.; Messina, F. Solvatochromism Unravels the Emission Mechanism of Carbon Nanodots. *J. Phys. Chem. Lett.* **2016**, *7* (17), 3419−3423.
(53) Bano, D.; Kumar, V.; Singh, V. K.; Chandra, S.; Singh, D. K.; Yadav, P. K.; Talat, M.; Hasan, S. H. A Facile and Simple Strategy for the Synthesis of Label Free Carbon Quantum Dots from the Latex of Euphorbia Milii and Its Peroxidase-Mimic Activity for the Naked Eye Detection of Glutathione in a Human Blood Serum. *ACS Sustainable Chem. Eng.* **2019**, *7* (2), 1923−1932.
(54) Chandra, S.; Singh, V. K.; Yadav, P. K.; Bano, D.; Kumar, V.; Pandey, V. K.; Talat, M.; Hasan, S. H. Mustard Seeds Derived Fluorescent Carbon Quantum Dots and Their Peroxidase-like Activity for Colorimetric Detection of H 2 O 2 and Ascorbic Acid in a Real Sample. *Anal. Chim. Acta* **2019**, *1054*, 145−156.
(55) Reichardt, C. Polarity of Ionic Liquids Determined Empirically by Means of Solvatochromic Pyridinium N-Phenolate Betaine Dyes. *Green Chem.* **2005**, *7* (5), 339−351.
(56) Reichardt, C. Solvatochromic Dyes as Solvent Polarity Indicators. *Chem. Rev.* **1994**, *94* (8), 2319−2358.
(57) Soares, M. C. P.; Gomes, M. K.; Schenkel, E. A.; Rodrigues, M. d. S.; Suzuki, C. K.; Torre, L. G. de la; Fujiwara, E. Evaluation of Silica Nanoparticle Colloidal Stability With a Fiber Optic Quasi-Elastic Light Scattering Sensor. *Braz. J. Chem. Eng.* **2019**, *36* (4), 1519−1534.
(58) Cannas, M.; Camarda, P.; Vaccaro, L.; Amato, F.; Messina, F.; Fiore, T.; Agnello, S.; Gelardi, F. M. Luminescence Efficiency of Si/SiO 2 Nanoparticles Produced by Laser Ablation. *Phys. Status Solidi A* **2019**, *216* (3), 1800565.
(59) Stephanopoulos, G. *Chemical Process Control: An Introduction to Theory and Practice*, 1st ed.; Prentice Hall: Hoboken, NJ, 1983.
(60) Skoog, D.; West, D.; Holler, F. J.; Crouch, S. *Fundamentals of Analytical Chemistry*, 9th ed.; Cengage Learning: Belmont, CA, 2014.
(61) Lakowicz, J. R. *Principles of Fluorescence Spectroscopy*, 3rd ed.; Lakowicz, J. R., Ed.; Springer: New York, 2006.
(62) Soares, M. C. P.; Vit, F. F.; Suzuki, C. K.; De La Torre, L. G.; Fujiwara, E. Perfusion Microfermentor Integrated into a Fiber Optic Quasi-Elastic Light Scattering Sensor for Fast Screening of Microbial Growth Parameters. *Sensors* **2019**, *19* (11), 2493.
(63) *pH Measurement Handbook*. Thermo Fischer Scientific Inc., 2020. https://assets.thermofisher.com/TFS-Assets/LSG/brochures/pH-Measurement-Handbook-S-PHREFBK-E.pdf (accessed 2020-09-13).
(64) *780 pH-Meter + 781 pH/Ion Meter*. Metrohm Ltd., 2010. https://partners.metrohm.com/GetDocumentPublic?action=get_dms_document&docid=692470 (accessed 2020-09-13).
(65) ASTM International. *Standard Test Method for pH of Aqueous Solutions With the Glass Electrode*; ASTM E70-19; ASTM International: West Conshohocken, PA, 2019.

https://doi.org/10.1021/acsanm.1c02127
ACS Appl. Nano Mater. 2021, 4, 9738−9751